High-Performance Abaqus Simulations in Soil Mechanics Reloaded – Chances and Frontiers

Torben Pichler, Tim Pucker, Thorben Hamann, Sascha Henke, Gang Qiu

Hamburg University of Technology (Germany), Institute of Geotechnical Engineering and Construction Management

Abstract: Abaqus is often used for soil mechanical purposes to solve complex boundary value problems. Simulations of geomechanical boundary value problems are rather complex because of the complexity of the material which incorporates stress dependent material behaviour or different stiffness for loading and unloading conditions for example. Furthermore, typical soil consists of three phases including the soil skeleton, pore water and pore air which lead to complex interaction. Moreover, the loading conditions typical in geomechanics often cause large deformations of the soil continuum which has to be considered in the choice of the appropriate calculation tool.
In this contribution several approaches are discussed to take into account the complexity of geomechanical boundary value problems. The complex soil behaviour is implemented via (V)UMAT user subroutines, first approaches for the implementation of the soil's two-phases via user elements or the constitutive behaviour respectively are demonstrated and the application of the explicit FEM-, CEL- and SPH-method for large deformation simulations is discussed.
The paper mainly focuses on the chances and frontiers our research group encountered during the last years of research dealing with high performance large deformation simulations in geomechanics under highly complex conditions.
Concluding, several examples of complex boundary value problems are presented. For example, the numerical simulation of screwed full displacement piles and the collision of a ship with the foundation of an offshore wind energy plant are discussed in detail.

Keywords: Abaqus, large deformation, CEL, SPH, FEM, soil mechanics, multi-phase material

1. Introduction – Special characteristics of the soil material

1.1 General comments

In contrast to steel or concrete the material behaviour of soils is rather complex. In general, it can be distinguished between granular (like sand and gravel) and soft soils (like clay). Therefore, in numerical simulations this complex material behaviour has to be taken into account. In this contribution the main focus lies on geomechanical boundary value problems mainly including granular material behaviour for the subsoil. Thus, in this section the typical behaviour of such material is discussed.

1.2 Composition of granular materials

Granular soils typically are a mixture consisting of three different phases, see Figure 1.

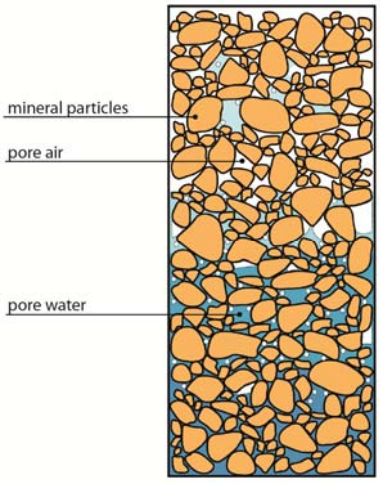

Figure 1. Granular material with three different phases.

- The soil skeleton consisting of mineral particles of different size and shape (Figure 1.),
- the pore water and
- the pore air which are located in the void regions between the grains.

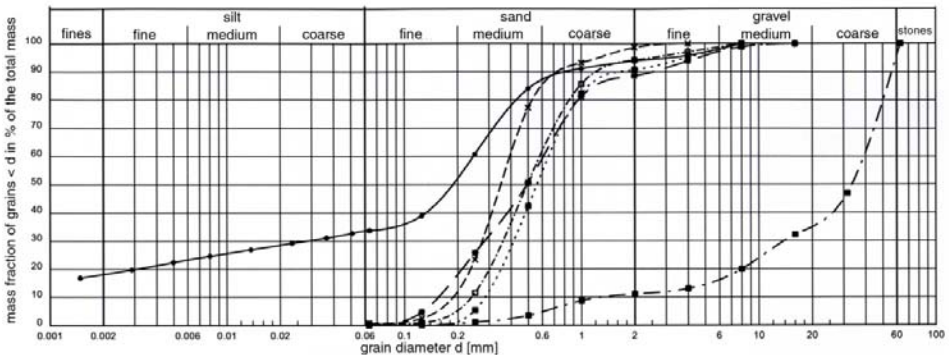

Figure 2. Example grain size distribution for different soils.

Under certain circumstances the material can be fully saturated such that the voids are completely filled with water, no pore air remains in the mixture. Otherwise in totally dry soil, no pore water is existent. In soil mechanics it is well known, that the material behaviour is strongly dependent on the degree of saturation. This will be discussed in more detail in Section 2.

1.3 Material behaviour of granular materials

The following characteristics are typical for granular materials like sand and gravel:

- Non-linear behaviour of the material,
- different stiffness for loading and unloading,
- dilatant or contractant behaviour of the material,
- dependency of the soil stiffness on the stress state,
- dependency of the soil stiffness on the void ratio or soil density respectively,
- anelastic behaviour and anelastic wave propagation under dynamic excitation, such that compaction of the soil occurs during cyclic shearing for example.

In soil mechanics and soil dynamics the behaviour of the soil typically is described by laboratory element tests like triaxial and oedometric tests for the mechanical properties under static loading and more complex element tests like dynamic shear or triaxial tests and resonant-column tests for dynamically loaded soil. As an example for these element tests the results of oedometric and triaxial tests for a granular material are depicted in Figure 3.

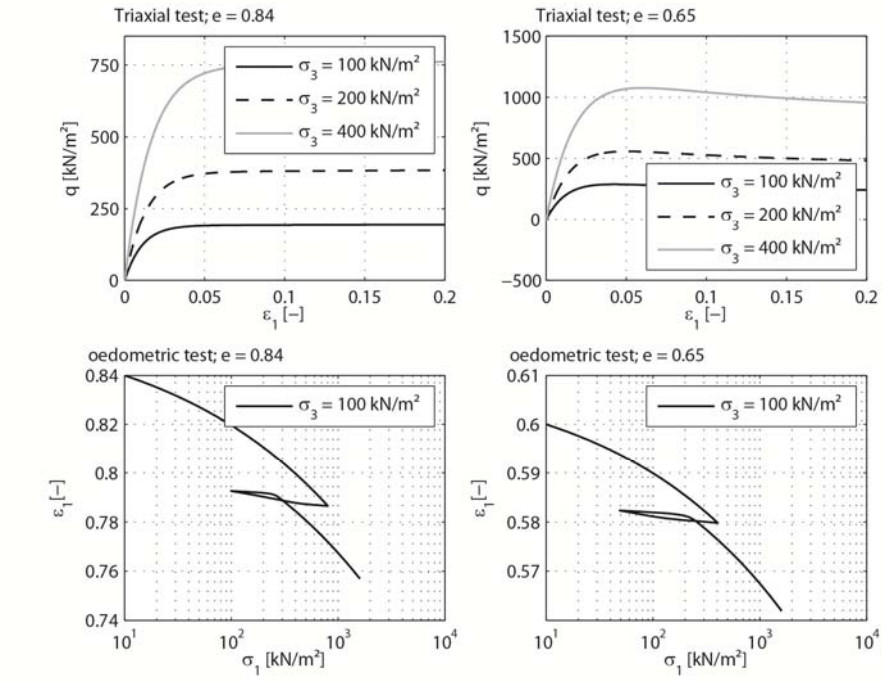

Figure 3. Exemplary results of oedometric and triaxial tests of granular material with different soil density and stress state.

1.4 Abaqus built-in analyses for soil mechanical purposes

Abaqus provides a wide range of tools to solve geomechanical boundary value problems:

- There are several different approaches to solve geomechanical boundary value problems, like **implicit Finite-Element-Method** (capable to solve small deformation boundary value problems with or without taking into account the pore water), **explicit Finite-Element-Method** (capable to solve boundary value problems with moderate to large deformations but limited to single-phase analyses) and the **coupled Eulerian-Lagrangian method** (capable to solve large deformation boundary value problems but also limited to single-phase analyses). In Abaqus 6.11 the **Smoothed Particle Hydrodynamics** is implemented which is not yet fully tested for geomechanical purposes.
- A number of **constitutive models for soils** are implemented in Abaqus like Mohr Coulomb plasticity, extended Drucker-Prager plasticity, modified Drucker-Prager/cap model and clay plasticity. All these models are rather conservative and do not incorporate typical soil characteristics like the dependency of the behaviour on the stress state and the void ratio or small-strain behaviour.
- Several **boundary conditions** can be defined. For dynamic simulations it is also possible to use infinite elements after Lysmer and Kuhlemeyer (1969) for classical FEM applications or absorbing boundaries for CEL analyses.
- With the `*INITIAL CONDITIONS` command it is possible to define the initial stress state, void ratio distribution or saturation for example.
- Further tools are different loads like gravity, distributed or concentrated loads. But it is also possible to define prescribed displacements.
- The `master-slave-principle` for the contact definition allows simulations with large deformations of a Lagrangian part which is typical for many applications in geomechanics.

1.5 Own extensions for soil mechanical purposes

- User defined subroutines can be implemented as `UMAT` and `VUMAT`. In this context it is possible to implement **constitutive models** which are better suited to describe the complex material behaviour of the soil. In the present contribution the behaviour of granular material is described using the hypoplasticity after Gudehus (1996) and von Wolffersdorff (1996) with the extension of intergranular strains after Niemunis and Herle (1997). Soft soil behaviour can be described with the visco-hypoplasticity after Niemunis (2003). Examples using the hypoplasticity in rather complex boundary value problems are discussed in Section 4.
- The behaviour of **multi-phase materials** cannot be described using the hypoplasticity without extension. It is for example possible to define a user defined element `(V)UEL` to describe the soil as a three-phase mixture with consideration of the soil skeleton, the pore water and the pore air in the numerical analyses. This has been shown by Schümann (2010) for example. Another approach is to describe the multi-phase behaviour of the

granular material by implementation in the framework of a (V)UMAT as it will be discussed in Section 2.

- User defined **contact models** can be defined with user subroutines (V)UINTER for the definition of normal and tangential contact behaviour whereas friction models are implemented using (V)FRIC, see Gutjahr (2003) and Arnold (2004) using hypoplastic contact models.

2. Soil as a multi-phase material

2.1 Introduction

Soil is a multiphase porous material that consists of mineral particles of different size and shape (solid phase) and voids which are filled with one or more fluids (fluid phase). The mineral particles build up the soil skeleton whose behaviour can be described by various constitutive models depending on the investigated target. In typical geotechnical problems the voids are filled with water and air, but also gas and oil are possible fluids for boundary value problems in reservoir engineering.

In typical geotechnical problems the load-bearing behaviour of the soil is significantly dependent on the pore water. To take the influence of pore water into account, the concept of effective stress (Terzaghi, 1944), given in Equation (1) is used, dividing the total stress $\boldsymbol{\sigma}$ of the mixture of soil and fluids into effective stress $\boldsymbol{\sigma'}$ acting on the solid skeleton and fluid pressure, see Lewis and Schrefler (2000):

$$\boldsymbol{\sigma} = \boldsymbol{\sigma}' - \boldsymbol{I}\left(\boldsymbol{S_w p_w} + \boldsymbol{S_g p_g}\right) \quad (1)$$

where $\boldsymbol{S_w}$ and $\boldsymbol{S_g}$ are the volume fractions of water and air regarding the volume of voids and p_w and p_g are the corresponding pressure. $\boldsymbol{I}$ is the second order unit tensor. In case of an external loading usually a relative motion between the individual phases occurs, so that there is an interaction between the constituents. It can be distinguished between fully drained, coupled and undrained conditions depending on the permeability of the soil and the velocity of load application. For fully drained conditions no excess pore water pressure occurs due to an immediate consolidation, when applying external loads. The influence of pore water can be neglected. In case of fully undrained conditions the soil is assumed to be impermeable or the velocity of load application is as high, that no consolidation of excess pore water pressure can take place. For fully coupled conditions a flow of the pore water can occur due to a gradient of pore water pressure, so that there is a time dependent behaviour of the soil due to consolidation.

Simple applications for fully coupled conditions, which can be dealt with the Abaqus built-in features, are the consolidation of a soil under static loading conditions, for example the development of settlements of a foundation or large embankment dams with respect to time. A more complex problem is the simulation of the behaviour of a water saturated soil under dynamic loading conditions for example earthquake loading or the vibratory driving of a pile. For loosely layered water saturated sands soil liquefaction can occur due to dynamic loading with the consequence of a loss of bearing capacity and large deformations. An analysis of such boundary value problems in combination with a hypoplastic material behaviour is not yet possible with the Abaqus built-in features. Also for boundary value problems dealing with large deformations,

which are usually solved, using the explicit Finite-Element-Method, the influence of pore water pressure cannot be taken into account. To avoid these restrictions regarding the explicit Finite-Element-Method, a first approach to describe the behaviour of a coupled two-phase material consisting of a fully saturated soil implemented in the framework of a VUMAT is presented in the following. The implementation of fully undrained conditions in combination with hypoplastic material models in the framework of user subroutines (V)UMAT has already been successful tested and can be found for example in Niemunis (2003) and Qiu (2011).

2.2 Implementation in the framework of a VUMAT

The user defined subroutine VUMAT is expressed in total stress of the mixture of solid and pore water. Using the concept of effective stress, a separation of total stress σ into effective stress σ' and pore water pressure p_w is done within the subroutine. The effective stress state and the pore water pressure are stored by the use of solution dependent variables (SDV). The stress-strain response is defined for both phases separately.

The constitutive behaviour of the solid skeleton is described with isotropic linear elasticity requiring two constants, which are the Young's modulus $\boldsymbol{E}$ and the Poisson's ratio $\boldsymbol{\nu}$:

$$\boldsymbol{\delta\sigma' = C\,\delta\varepsilon} \quad (2)$$

where $\boldsymbol{C}$ is the stiffness matrix of the solid skeleton.

Modelling the behaviour of the pore water phase a mass balance equation is introduced (Lewis and Schrefler, 2000):

$$\boldsymbol{\frac{n}{K_w}\frac{\partial p_w}{\partial t} + \mathbf{div}(v_s) + \mathbf{div}(n v_{ws}) = 0} \quad (3)$$

where $\boldsymbol{n}$ is the porosity, $\boldsymbol{K_w}$ the bulk modulus of pore water, $\boldsymbol{v_s}$ the velocity of the solid skeleton and $\boldsymbol{v_{ws}}$ the relative velocity between the pore water and the solid skeleton. The solid grains are assumed to be incompressible. Obtaining the relative velocity of pore water, Darcy's law for fully saturated conditions is introduced:

$$\boldsymbol{n v_{ws} = \frac{k_f}{\gamma_w}[-\mathbf{grad}(p_w) + \rho_w g]} \quad (4)$$

where $\boldsymbol{k_f}$ is the permeability of a fully saturated medium, $\boldsymbol{\gamma_w}$ the specific weight of pore water, $\boldsymbol{\rho_w}$ the density of pore water and $\boldsymbol{g}$ the gravitational acceleration.
Any time Abaqus calls the user subroutine and provides a new strain increment, a new effective stress state and a new pore water pressure is computed within the subroutine and a new total stress state is returned to Abaqus.

The main limitation of this approach is the determination of the gradient of pore water pressure, which is stored as a SDV for each finite element. For a certain element the gradient of the pore water pressure can be approximated within the user subroutine with the knowledge of the pore water pressure of the neighbouring elements, the area of the interacting surface to the neighbouring elements and the distance to the neighbouring elements.

2.3 Validation

To validate the implemented approach an axisymmetric oedometric test under static loading conditions is simulated with Abaqus/Explicit. The results are compared to a coupled pore fluid

diffusion and stress analysis carried out with Abaqus/Standard. The geometry and boundary conditions of the discretized model are shown in Figure 4. The oedometric test has a height of 2 m and a diameter of 4 m. The lateral and bottom surface are fixed in its displacement normal to the surface and are impermeable regarding a fluid flow. At the upper surface a pressure is defined and the pore water pressure is set to zero. The soil body is discretized with 1000 four-noded continuum elements with reduced integration and hourglass control. To obtain a smoothed pore water pressure distribution over the height of the oedometric test, a fine discretisation with an element height of 2 cm is used. The chosen material parameters are given in Table 1. In the first step of the analyses with a time period of 1 s, the gravity with $g = 10\ \mathrm{m/s^2}$ and a surface pressure of $p = 10\ \mathrm{kN/m^2}$ is defined. The corresponding stress state and pore water pressure is specified by initial conditions to obtain an undeformed initial state. During the second step ($1\ \mathrm{s} \leq t \leq 11\ \mathrm{s}$) the surface pressure is increased linearly up to $1000\ \mathrm{kN/m^2}$. In the last step ($11\ \mathrm{s} \leq t \leq 21\ \mathrm{s}$) the external loads remain unchanged and consolidation can take place.

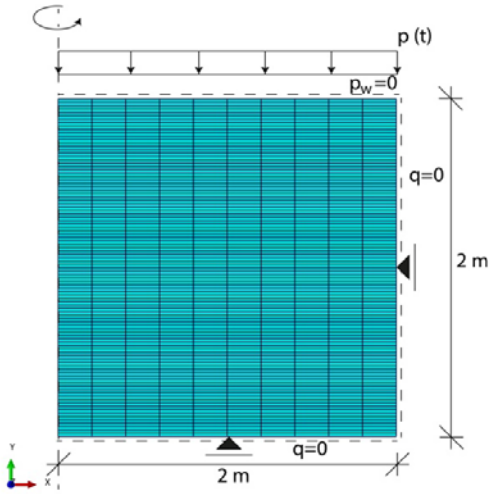

Figure 4. Model of the discretized oedometric test with geometry and boundary conditions.

Table 1. Soil parameters for the coupled pore fluid diffusion and stress analyses.

Parameter		Value
E	Young's modulus of solid skeleton	$30{,}000\ \mathrm{kN/m^2}$
ν	Possion's ratio	0.3
K_w	bulk modulus of pore water	$2.0 \cdot 10^6\ \mathrm{kN/m^2}$
k_f	permeability	$5.0 \cdot 10^{-6}\ \mathrm{m/s}$
e	initial void ratio	0.66
ρ_w	density of pore water	$1.0\ \mathrm{t/m^3}$

In Figure 5 the pore water pressure distribution over the height of the oedometric test is shown for different simulation times. The implemented approach using a total stress analyses fits very well with the solution obtained from Abaqus/Standard under the precondition of a sufficiently fine discretization and a one-dimensional consolidation. A comparison of the calculated vertical deformation of the upper surface of the soil body with respect to time also shows a good agreement with the Abaqus/Standard solution, see Figure 6.

The presented approach is one approach to carry out coupled pore fluid diffusion and stress analyses with Abaqus/Explicit to investigate boundary value problems with large deformations or dynamic loadings. For static loading this approach provides good results. One of the main limitations for the implementation of this approach is the complicated determination of the gradient of the pore water pressure, because Abaqus provides no built-in function to obtain the gradient of a SDV.

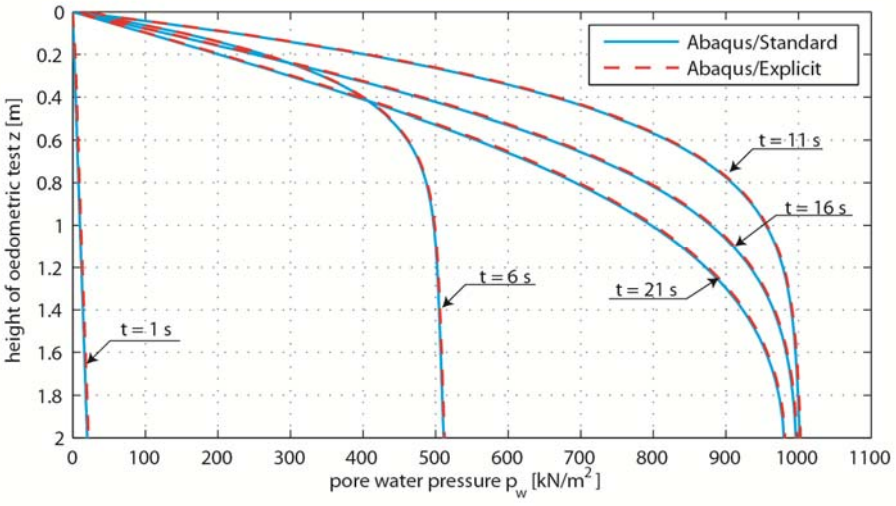

Figure 5. Distribution of the pore water pressure over the height of the oedometric test.

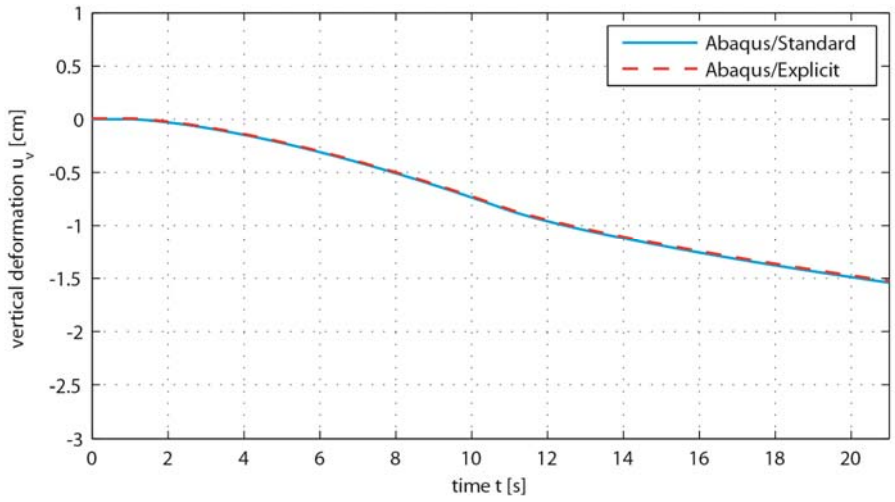

Figure 6. Vertical deformation of the upper surface with respect to time.

3. Large deformation analyses in Geomechanics

The Finite-Element-Method has been widely used to solve geotechnical problems. According to Mair (1979), the range $0.01\ \% - 1\ \%$ strain encompasses serviceability and pre-failure deformations. Thus, the applications of FE method to design the retaining wall systems and foundations belong to small deformation analyses. For the problems such as pile installation, punch test and ship grounding the soil-structure interface experiences large deformations. The frictional contact between soil and structure becomes complicated. The soil can be separated from the structure and the gaps may be re-closed later.

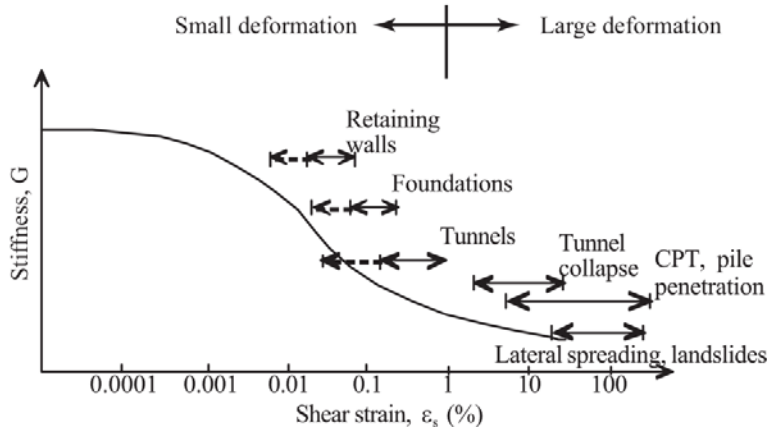

Figure 7. Typical strain range experienced in geotechnical engineering, modified from Mair (1979).

By solving boundary value problems such as pile penetration, punch test and ship grounding the soil experiences large deformations and the large deformation theory should be used in the numerical analyses. The large deformation theory, sometimes called large strain theory or finite strain theory, deals with deformations in which both rotations and strains are arbitrarily large. In the large deformation analyses, it is more convenient to use the deformation gradient tensor **F** and the deformation tensor **C** than the displacement gradient tensor **H** and the strain tensor **E**. Furthermore, the conventional strain tensor and engineering stress are usually used in small deformation analyses, whereas the logarithmic strain tensor and Jaumann rate of Cauchy stress are preferred in the large deformation analyses.

In the large deformation analyses, large deformations may result in large changes in the aspect ratio of elements and material failure may lead to generate new free surface (e.g. by pile penetration). A converged solution cannot be obtained. Thus, some numerical methods, such as Arbitrary Lagrangian-Eulerian method (ALE), Coupled Eulerian-Lagrangian method (CEL) and Smoothed Particle Hydrodynamics (SPH), which can overcome the mesh distortion problem, have been implemented in Abaqus to solve boundary value problems. In the following section, several geotechnical boundary value problems are solved by using the explicit, CEL or the SPH methods.

4. Example simulations

4.1 Collision of a ship with a gravity base foundation – FEM

4.1.1 Introduction

For the installation of offshore foundations Germany demands proof, that in case of a collision with a vessel neither a discharge of supplies nor the loss of the vessel occurs. This was investigated by Biehl (2008) for steel structures like monopiles, tripods and jackets. Due to their small stiffness compared to the vessels stiffness these structures generally fail without damaging a vessel severely. Because of the stiffness of gravity base structures greater damage to the vessel is to be expected. The Finite-Element-Method provides the capabilities to investigate the collision behaviour of the steel vessel, the concrete structure and the supporting soil.

In the simulations presented a collision between disabled single hull tanker and a gravity base structure for a 6 MW offshore wind turbine is assumed as a worst case scenario. The foundation is shown in Figure 8 and a cross section of the single hull tanker is displayed in Figure 9.

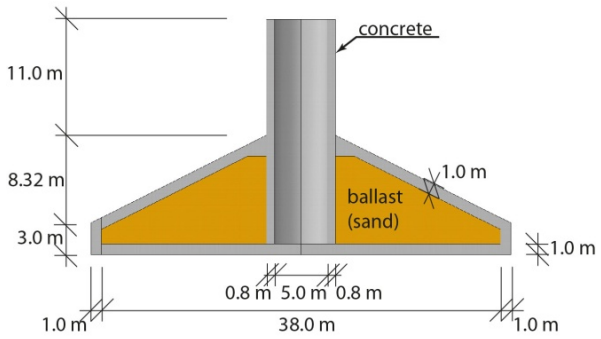

Figure 8. Geometry of the gravity base foundation.

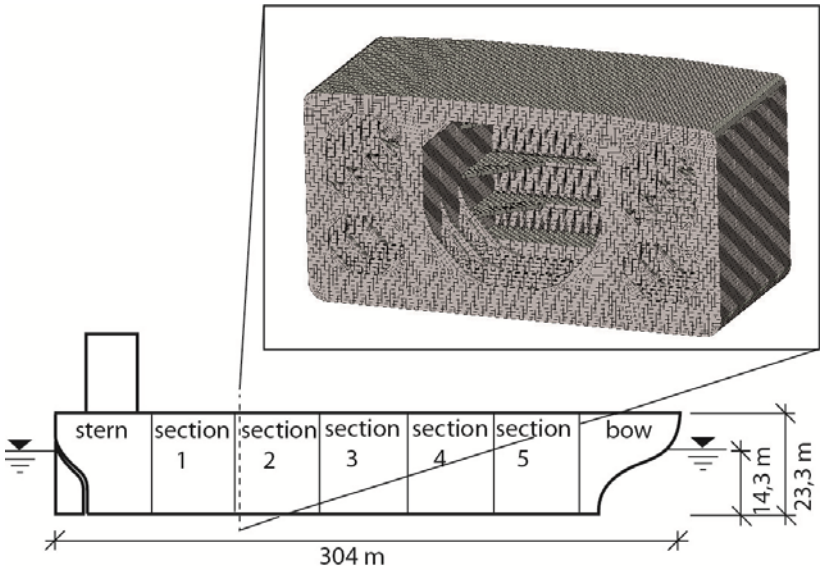

Figure 9. Sketch of the single hull tanker with the cross section of a ship section.

4.1.2 Numerical Modelling

Three dimensional dynamic analyses with explicit time integration where performed using Abaqus/Explicit 6.10. The influence of pore water, wind and wave loading was not considered here, since Abaqus/Explicit provides no build-in tools for pore water calculation and wind or wave loading is not controlling.

The underlying single hull tanker has a mass of 200,000 t, a length of 304 m, a width of 46 m and a height of 23.3 m. It consists of five identical ship sections, stern and bow. The soil and the foundation are discretised with deformable 8-node continuum elements. The soil body has a diameter of 200 m and a height of 80 m. The tower is discretised with 100 mm thick 4-node shell elements and the nacelle is idealised as a mass point of 430 t. Because of the symmetry only half of the model is simulated. Figure 10 depicts the finite element model. The interaction between the foundation and the tower as well as the tower and the nacelle is carried out by kinematic coupling of all degrees of freedom.

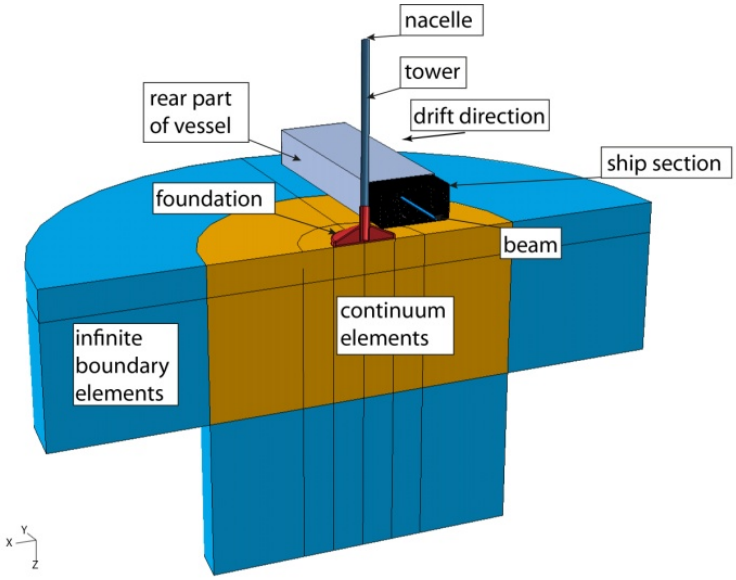

Figure 10. Numerical model for the simulation of ship collision.

The model of the vessel is simplified, only one half of a section is modelled in respect to the calculation time. To account for the buoyancy a rigid beam is placed in the vessels longitudinal axis. The beam takes over the bearing of the vessel by use of kinematic coupling of the transverse bulkheads. The beam is held in vertical direction and rotatable in its axis with a torsion spring to simulate self-aligning torque in case of rotation during the sliding onto the gravity base structure.

The constitutive model after Mohr-Coulomb with elastic, ideal plastic material behaviour is used for soil and concrete. The material behaviour of the tower and the ship section is described by a linear elastic Mises material with an isotropic hardening and softening plasticity by specifying the stress-strain behaviour of a steel S235. The material parameters used are given in Table 2. The nacelle, the stern of the vessel and the beam are modelled as rigid bodies.

Table 2. Material parameters for simulation of ship collision.

Parameter		**sand**	**concrete**	**steel**
γ / γ' [kN/m^3]	unit weight / submerged unit weight	19 / 9	25 / 15	78.5 / 68.5
E [kPa]	Young's modulus	30,000	$3.6 \cdot 10^7$	$2.1 \cdot 10^8$
ν [1]	Possion's ratio	0.3	0.2	0.3
φ' [°]	effective angle of friction	30	63.2	–
ψ [°]	dilatancy angle	0	0.1	–
c' [kPa]	cohesion below the water table	0	5,353	–

4.1.3 Results of collision simulation

A cross section of the simulated scenario is shown in Figure 11. Figure 12 gives the computed result of the horizontal contact force between ship and gravity base foundation and a simplified approximation. The simplified approximation is the maximum frictional force between foundation and soil.

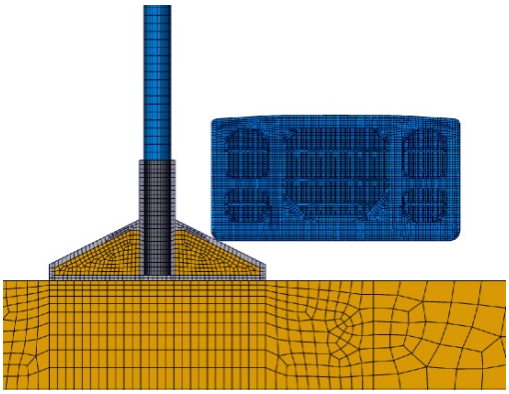

Figure 11. Investigated scenario.

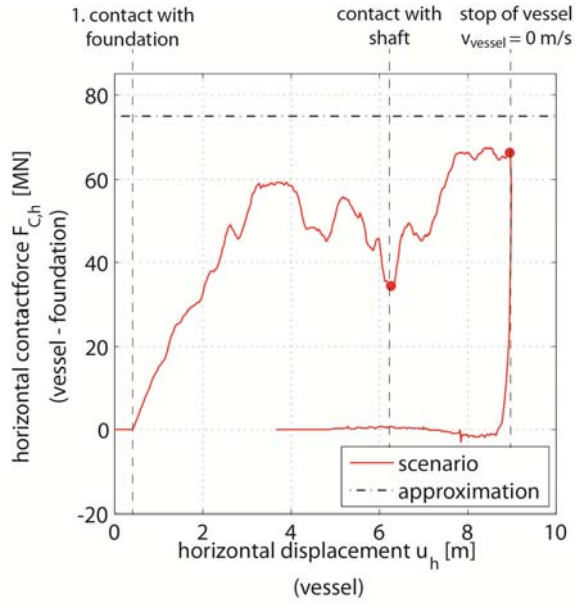

Figure 12. Comparison of the contact force to a simplified engineering approximation.

The collision process can be divided into three phases. The first phase is the sliding onto the cone of the foundation and the deceleration of the vessel. The horizontal contact force is rising up to 60 MN. In the second phase the vessel gets in contact with the shaft of the foundation and the contact force increases up to 68 MN, but the approximated upper limit of 75 MN is not achieved. In the third phase, the vessel drifts back from the foundation. The contact force is reduced to zero. Figure 13 shows the dissipation of the kinetic energy during the simulation. Even though most of the kinetic energy is dissipated by friction, still about 33 % is dissipated by plastic deformation of the vessel.

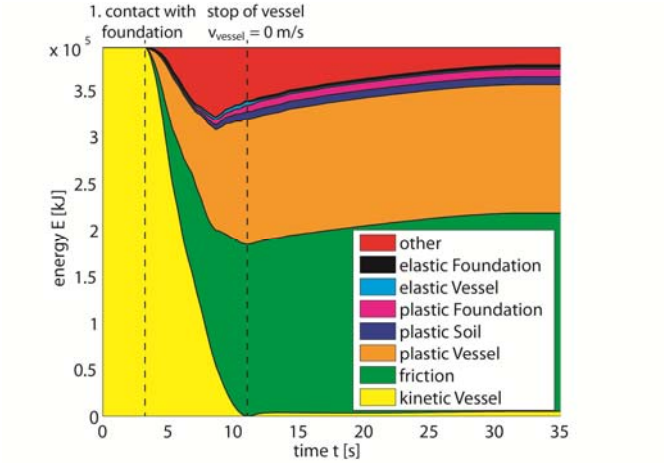

Figure 13. Distribution of energy during simulation of collision.

4.1.4 Deformation and damage of the vessel

For the evaluation of the collision behaviour the calculated deformation of the vessel and the damage of the vessel's hull are investigated. The vessel is severely deformed in a locally limited area and the outer hull is folded a little. To evaluate the damage of the vessel the fracture criterion developed by Yu (1997) is used. The failure of an element is calculated as a function of the current stress and strain state and the size of an element. The strain of steel ε_t is multiplied by a factor taking into account the stress state and is compared with a critical strain according to Equation (5). The critical strain $\varepsilon_{\mathrm{crit}}$ is given by Equation (6) and takes into account the thickness and length of an element. A fracture occurs if the critical strain is exceeded. The parameters for Equation (5) and (6) are shown in Table 3.

$$\varepsilon_t \left(\frac{2}{2}(1+\nu) + 3(1-2\nu)\left(\frac{\sigma_h}{\sigma_v}\right) \right) \geq \varepsilon_{crit} \quad (5)$$

$$\varepsilon_{crit} = \varepsilon_g + \alpha \frac{t_{sheet}}{l} = 0.08 \quad (6)$$

Table 3. Parameters for fracture criterion.

$\varepsilon_g = 0.056$	strain before reduction in area
$\alpha = 0.54$	coefficient
$t_{sheet} = 20$ mm	sheet thickness
$l = 0.45$ m	element length

According to this failure criterion areas of large deformation, in which a failure of steel is calculated, are shown in Figure 14 (red) on the undeformed vessel. Failure areas occur only locally limited in the deformed area. The total failure area of the outer hull of the vessel is approximately 4.9 m^2.

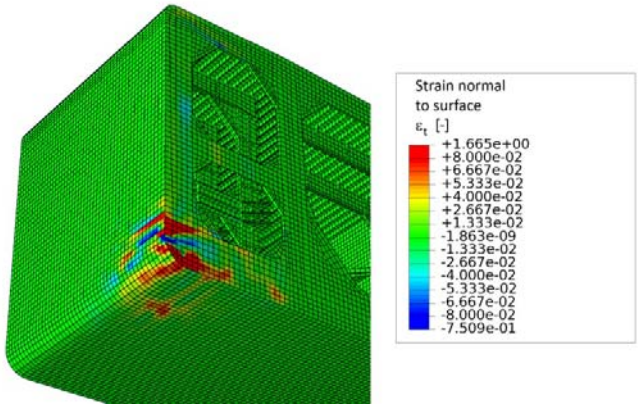

Figure 14. Damage of the vessel's hull after collision.

4.1.5 Conclusion

To investigate the collision behaviour of a gravity base structure, a collision between the fixed structure and a disabled single hull tanker is simulated numerically, using the Finite-Element-Method. The horizontal contact force between vessel and foundation is calculated in the simulation and compared to a simplified calculation approach. For evaluation of the collision behaviour of the foundation the deformation and damage of the vessel is calculated. The simplified calculation approach, as shown in Figure 12 as a constant value, leads to an overestimation of the horizontal contact force caused by neglecting the dissipation of the kinetic energy of the vessel by elastic and plastic deformation, in particular of the vessel. The finite element simulation gives a much better prediction of the contact forces. In the simulations the maximum of the contact force occurs at the time, when the vessel gets in contact with the shaft of the foundation.

The carried out simulations show, that a simple and cost effective investigation of the collision process is possible using the Finite-Element-Method. The design of a gravity foundation can be optimized regarding ship collision by variation of selected parameters using this method.

4.2 Installation of screwed piles – CEL

4.2.1 Introduction

Pile foundations are an important type of foundation in geotechnics. They are used to transfer building loads through soft soils into stable soil layers. Typical application examples are bridges, quay wall structures, skyscrapers or offshore wind turbines.

The installation process of piles influences the surrounding soil depending on the installation method. The piles can be driven, jacked, vibrated or drilled into the ground. The effects inside the soil are still not completely investigated. Therefore, most methods to predict the pile behavior or its bearing capacity are based on empirical approaches.

The influences of the installation process on the surrounding soil have been investigated for driven, jacked and vibrated piles by Mahutka (2007), Henke (2008), Henke and Grabe (2009) in numerical studies. In this section, the numerical simulation of the installation process of drilled piles is presented. Using this simulation, new insight can be gained in understanding effects in the soil nearby installed piles. The installation of a full displacement pile with lost bit (FDP) is simulated. Full displacement piles push the soil sideways without excavating soil. The installation process is divided into six steps schematically presented in Figure 15.

In the first step the drilling tool is taken into position. During the second and the third step, the drilling tool is drilled to the purposed depth. During the drilling process, the soil is transported to the displacement body where the soil is compacted. The reinforcement basket is installed in step four. The drilling tool is removed in step five and the pile is concreted simultaneously. The concrete hardens in step six and the installation is completed. The presented numerical study simulates only the steps two and three. A detail of the drilling tool is illustrated in Figure 16.

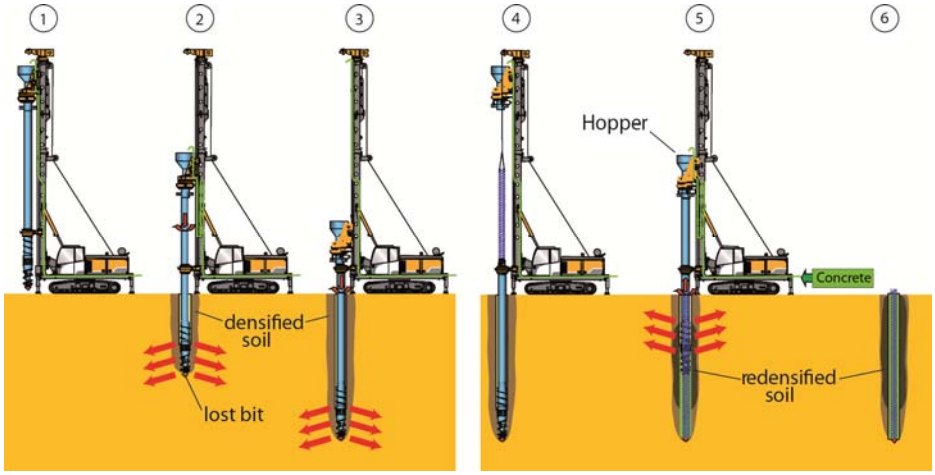

Figure 15. Schematic illustration of the installation process of full displacement piles (Busch et al., 2010).

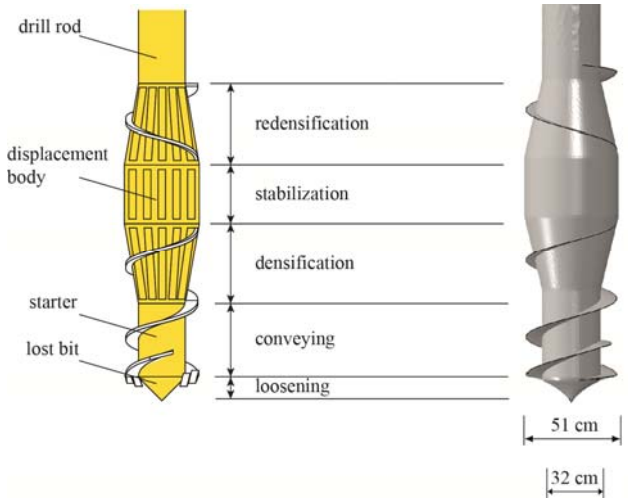

Figure 16. Scheme of the FDP drilling tool invented by BAUER (Busch et al., 2010) (left); numerical discretization of the drilling tool (right).

4.2.2 Numerical simulation

Modeling

Due to the asymmetric drilling tool and the applied CEL-Method, a three dimensional model has to be used. The drilling tool is modeled as a rigid body, because it is assumed, that the

deformations of the drilling tool a neglectable according to the large deformations of the soil. The displacement body has a diameter about 51 cm and the drill rod about 32 cm. The diameter of the auger elements relate to the displacement body.

The soil is modeled as an Eulerian area. The shape is cylindrical with a diameter about 16 m and a height of 20 m. Thereby, the distance between the boundaries and the drilling tool is more than 15 D (15 times of the pile diameter D), so that no influences of the boundary conditions on the results are expected. Above the soil, a 2 m void area is provided, so that the soil can avoid into this free space during the drilling process. The whole Eulerian area is discretized with approx. 163,000 eight-noded elements with reduced integration. The discretized model is shown in Figure 17.

The drilling tool penetrates the soil velocity controlled. Assuming, that the response of the soil model does not depend on the velocity, the penetration velocity is taken to 1 m/s. The ratio between the penetration velocity and the rotation velocity should be approx. 10. Therefore the rotational velocity is chosen to 10 U/s. The reaction forces and moments are recorded during the simulation.

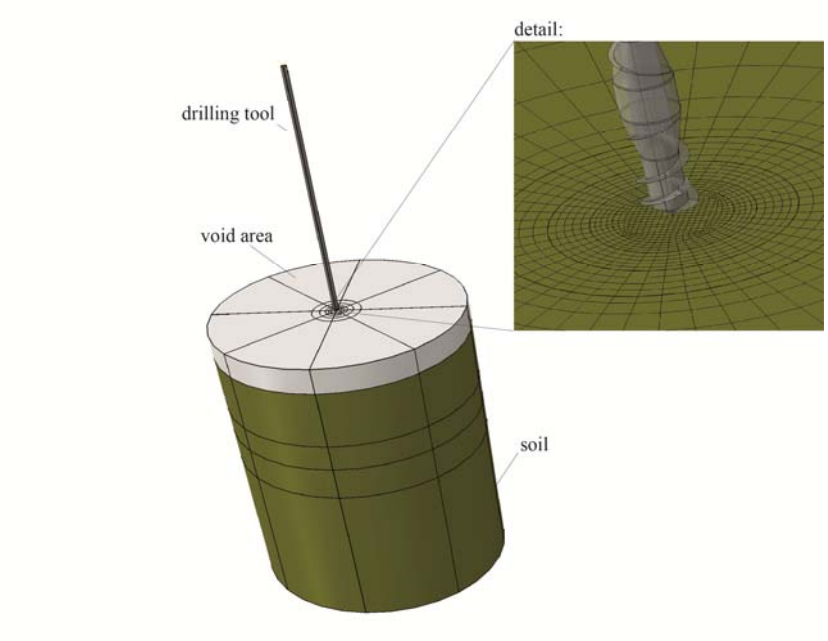

Figure 17. Discretized model with void area and mesh of the soil in detail.

Contact

The general contact algorithm is used. The normal contact is chosen to hard contact and the tangential contact uses the Mohr-Coulomb model with a friction angle about $\delta = \frac{1}{3}\varphi'$.

Constitutive model

The hypoplastic constitutive model presented in section 1.5 is used to simulate the drilling process. The material is chosen as Mai-Liao sand and its parameters are given in Table 4.

Table 4. Soil parameters for Mai-Liao sand for the hypoplastic constitutive model.

Material	φ [°]	h_s [MN/m²]	n [1]	e_{d0} [1]	e_{c0} [1]	e_{i0} [1]	α [1]
Mai-Liao sand	31.5	32.0	0.324	0.75	1.04	1.20	0.40

Material (continuance)	β [1]	m_T [1]	m_R [1]	R [1]	β_R [1]	χ [1]
Mai-Liao sand	1.00	2.00	5.00	0.0001	0.50	6.00

4.2.3 Results

Changes of the stress state

The stress state around the drilling tool is significantly influenced, see Figure 18. The transport of the soil to the displacement body causes a compaction of the soil at the height of the displacement body. After the displacement body passes through, a gap between the soil and the drill rod occurs and the soil can relax. Therefore, the horizontal stresses, illustrated in Figure 18, decrease nearby the drilling tool. The massive compaction of the soil in combination with the changing cross-section of the drilling tool leads to a reduction of the horizontal stresses nearby the drilling tool.

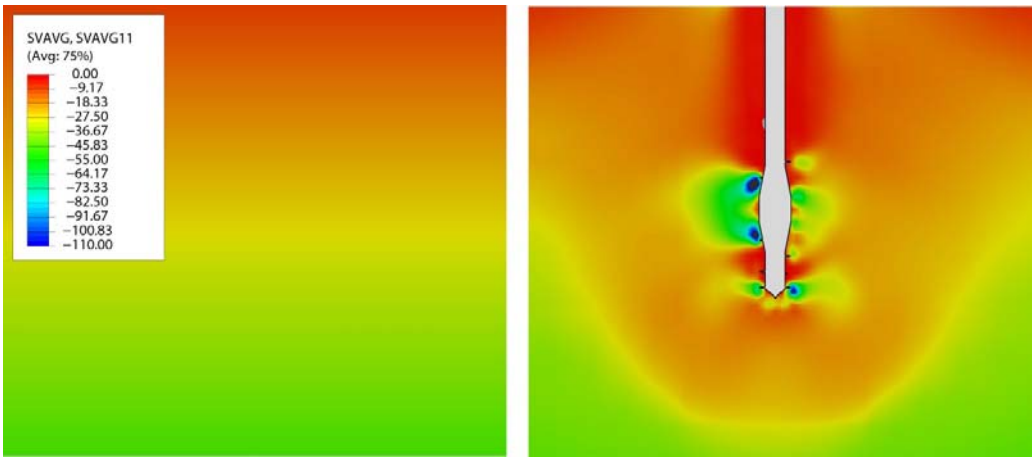

Figure 18. Horizontal stresses in the soil before (left) and after the drilling process (right).

Changes of the soil's bulk density

The hypoplastic constitutive model is able to predict changes of the soil's bulk density, see section 1.5. These changes caused by the drilling process are shown in Figure 19. The influence of two different velocity ratios between the penetration velocity v_z and the rotation velocity v_r are investigated. Nearby the drilling tool, the soil is loosened up, caused by the changing cross-section of the drilling tool. Between a distance of 1 D to 3 D, the soil is strongly densified.

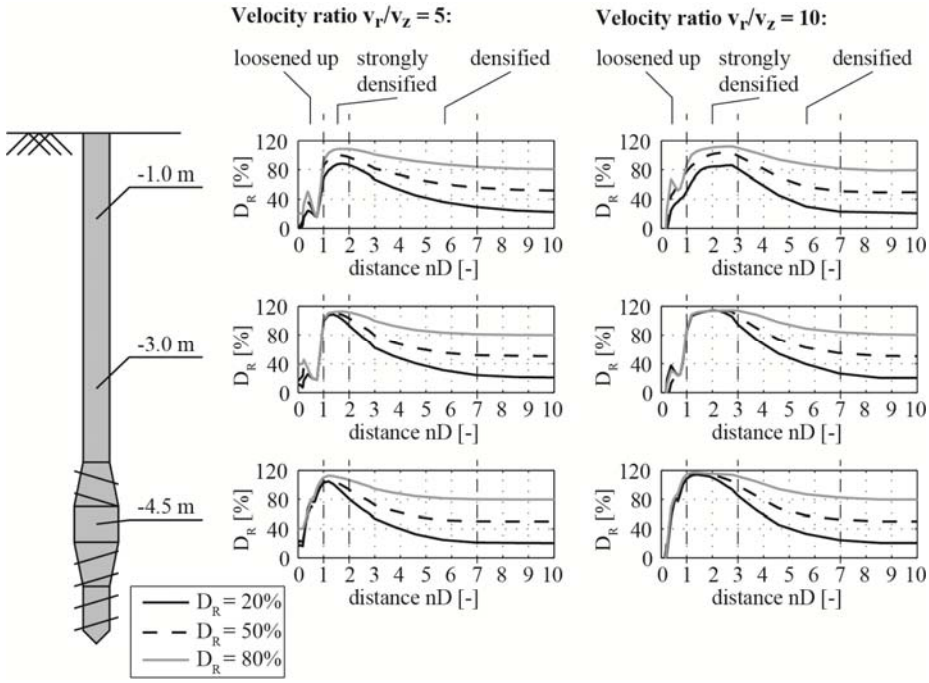

Figure 19. Bulk density of the soil along horizontal paths at depths of 1 m, 3 m and 4.5 m after completion of the 6 m drilling process for different drilling ratios.

4.2.4 Conclusion

The CEL-method is able to reproduce the soil's behaviour during a drilling process. The changes of the stress state and of the bulk density can be investigated. Therefore, this method can be used to gain deeper insights into the soil behaviour and the influencing installation parameters, such as the penetration and rotation velocity as well as the geometric properties of the drilling tool.

4.3 Numerical simulation of the deep penetration process of spudcan foundation into sand overlying clay – CEL

For oil drilling and gas well operations in deep water offshore jack-up rigs are often used. Punch-through failure may occur during operation in certain ground conditions (sand layer over soft clay), which may lead to damage or loss of the jack-up. The footings of jack-up rigs are known as spudcan foundations. The most widely used methods to predict the bearing capacity of a spudcan in practice are the punching shear method and the projected area method. In these methods, an imaginary sand block is assumed in shape of a column or a frustum being pushed into the underlying clay. The bearing capacity of the layered soils is obtained from the force equilibrium of the sand block. In the projected area method, the shear strength of the sand is neglected. The understanding of the failure mechanisms of soil underneath spudcan foundations is not sufficient, when a spudcan is penetrating into the soil.

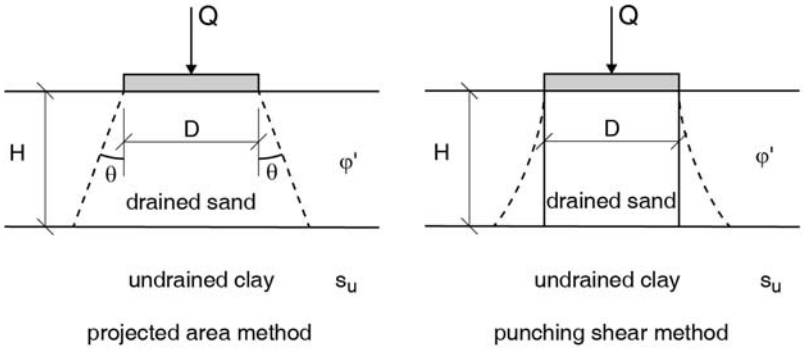

Figure 20. Failure mechanisms of the projected area method and punching shear method.

In the numerical simulations, the Coupled Eulerian-Lagrangian method is used. The sand is modeled under drained condition by using the hypoplastic model (von Wolffersdorff, 1996), whereas the clay is modeled under undrained condition by using the visco-hypoplastic model (Niemunis, 2003). The soil parameters have been determinated by Qiu and Grabe (2012b). The roughness factor $\alpha = 0.5$ is adopted in the simulation. The centrifuge test T2 (Teh et al., 2008) has been back-calculated. The calculated bearing resistance is in good agreement with the test result (Qiu and Grabe, 2012a). The failure mechanisms due to the penetration of a spudcan into dense sand overlying clay are illustrated by plotting the deviatoric strain rate. Following failure mechanisms can be observed:

(a) Just after the cone is completely penetrated into the sand, a vertical shear band and curved shear band spreading outwards can be observed. It looks the same as the punching shear failure suggested by Meyerhof (1978).

(b) At this state, several inclined shear bands can be observed. The inward and outward inclinations of the shear bands have the same angle of about $20°$ to vertical. A rigid sand plug with sidewall tapered inwards is pushed into clay, beside which a fan-shaped failure body is pushed radically outwards.

(c) The further penetration leads to reduction of the height of the fan-shaped sector, which is limited to the sand-clay interface.

(d) With the reduction of the height of the sector, the friction between the two failure bodies becomes less. The sand plug changes his form back to a cylinder. The failure mechanism keeps then unchanged and the cylindrical sand plug is pushed into the clay.

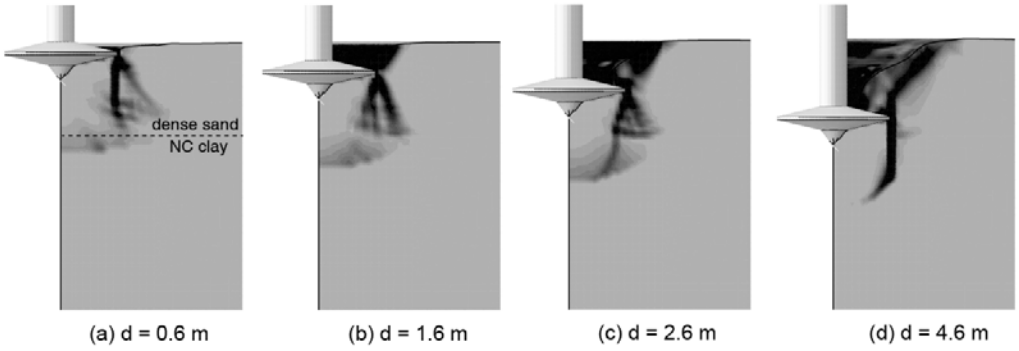

Figure 21. Development of the shear band in following the penetration of a spud-can into dense sand overlying clay (Qiu and Grabe, 2012b).

In further research work, a numerical parametric study is carried out by Qiu and Henke (2011) to simulate the penetration of a spudcan into loose sand overlying clay. The bearing capacity increases with increasing sand layer thickness, sand friction angle and clay shear strength. Most important, the peak value of the resistance q_{peak} can be expressed by the linear equation

$$q_{peak} = f\eta \,. \quad (7)$$

The empirical constant f is only dependent on the stiffness of the loose sand in-site and the geometryof the spudcan. The properties of clay and the sand thickness have no remarkable influence on f. Based on the relationship between q_{peak} and η, an idea for a possible in-situ measurement concept is suggested to control the installation of spudcan foundations founded on loose sand overlying weak clay, see Figure 22.

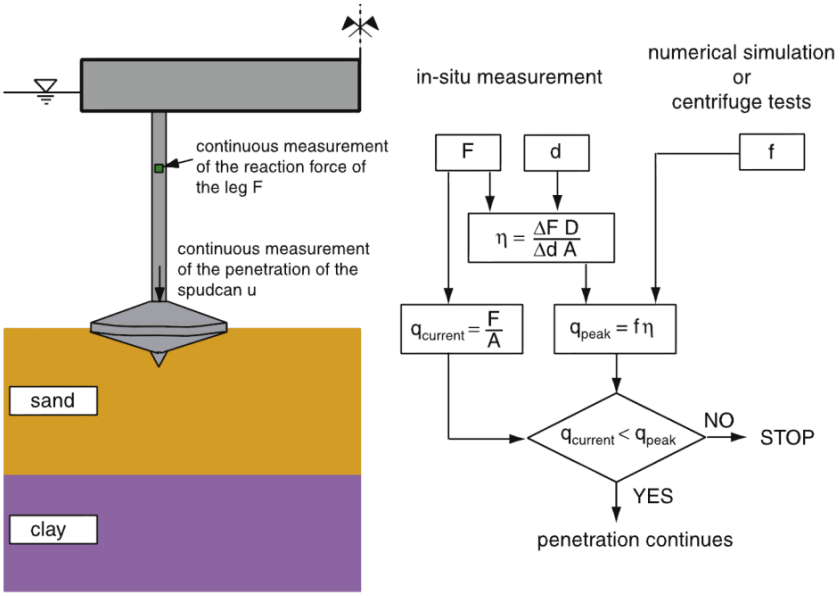

Figure 22. A concept to control the penetration process of jack-up platforms (Qiu and Henke, 2011).

4.4 First application of Smoothed Particle Hydrodynamics in soil mechanics – SPH

4.4.1 Benchmark problem

To evaluate the capabilities of the SPH a strip-footing benchmark has been simulated, see Figure 23.

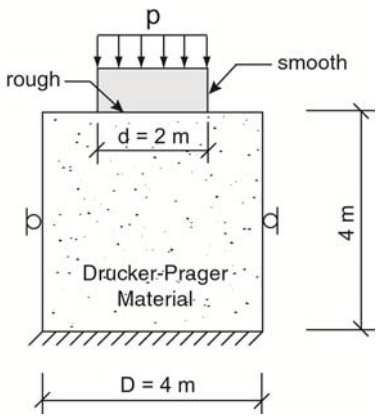

Figure 23. Strip-footing benchmark.

In this benchmark, a rigid footing (width: 2 m) is pressed into a 1 m long soil continuum with the dimensions 4 m by 4 m. The material for the soil is the Drucker-Prager material with a friction angle of 0° and a cohesion of $c = 10\ \mathrm{kN/m^2}$. The footing's base is rough whereas the lateral faces are modelled as smooth.

The analytical solution for this problem is given by Hill (1950):

$$p = (2 + \pi)c \quad (8)$$

The numerical model consists of 21,600 equidistant particles. Due to symmetry only half of the model is discretized, see Figure 24. The footing penetrates into the soil with a constant velocity of $0.05\ \mathrm{m/s}$. A vector plot of the resulting velocities after 0.5 m penetration of the footing is depicted in Figure 25.

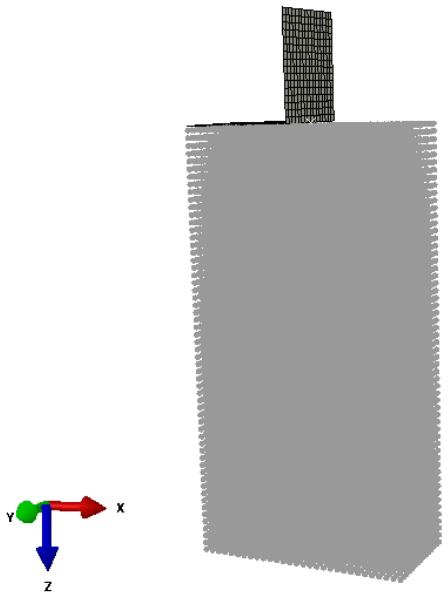

Figure 24. Discretization of the strip-footing benchmark with 21,600 particles.

The resulting fracture mechanism fits to results shown in Hill (1950) for example. Furthermore, Qiu et al. (2011) carried out a numerical study of the same benchmark analysed using different numerical approaches (implicit and explicit FEM and CEL). Especially, the CEL results are in good agreement to the velocity field shown in Figure 26.

The results of the study of Qiu et al. (2011) can be seen in Figure 26.

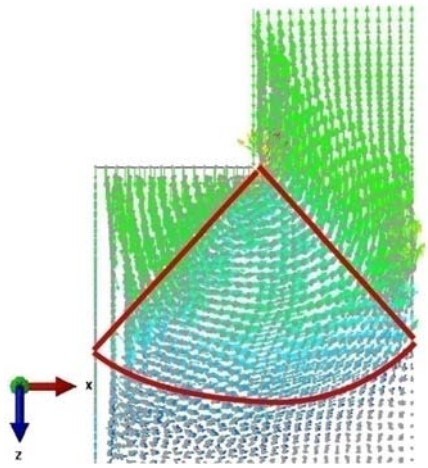

Figure 25. Vector plot of the resulting velocities after 0.5 m penetration of the footing into the subsoil.

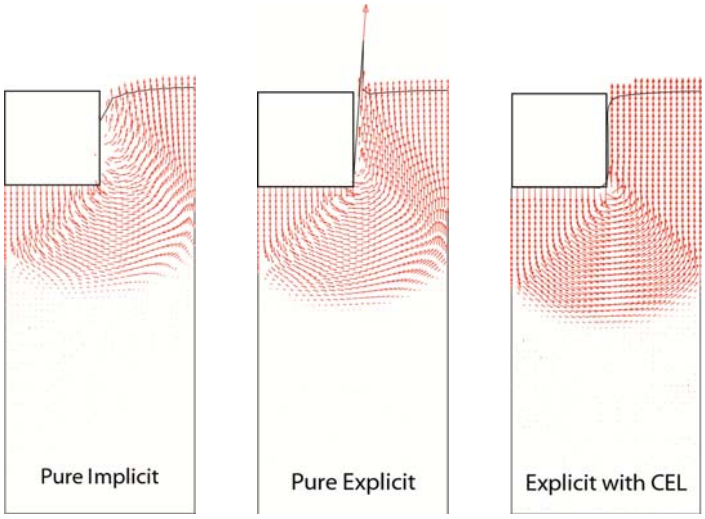

Figure 26. Velocity fields after 0.5 m penetration of the strip footing into the subsoil out of a simulation using Abaqus/Standard (left), Abaqus/Explicit (centre) and Abaqus/CEL (right), see Qiu et al. (2011).

In Figure 27 the normalized penetration resistance of the SPH- and CEL-result is compared to the analytical solution in Equation (1). It can be concluded that both the CEL and the SPH-solution

have similar quality such that the SPH- method seems to be suitable to be used for more complex geomechanical boundary value problems.

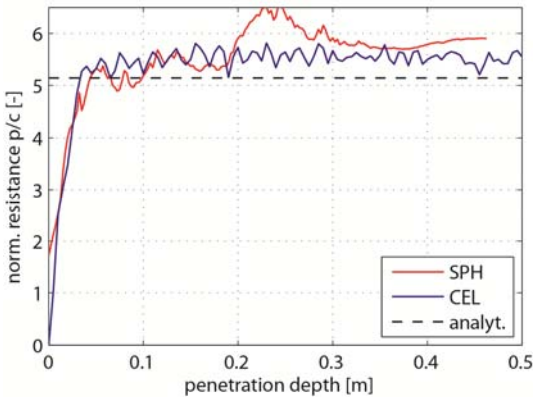

Figure 27. Normalized penetration resistance of the foundation compared to the analytical solution.

4.4.2 Pile installation

Numerical model

A first application of the SPH-Method in geotechnics has been performed on an exemplary pile driving process. A circular pile is penetrated into a cylindrical soil body up to an installation depth of about 5 m. The pile diameter is 1 m and the soil body diameter is 4 m. The height of the soil body is 10 m, see Figure 28. The pile is modelled as a rigid body and the soil as Mai-Liao sand using the hypoplastic constitutive model, see section 1.5. The reaction force of the pile is recorded during the simulation. Three different discretizations of the model are investigated. A coarse discretization with 11,562 particles, a fine one with 78,651 and a very fine one with 1,208,010 particles are created. The results of these calculations are compared to similar CEL-calculations. The same model is simulated with the CEL-Method and the discretization is equal to those of the SPH-models, except a void area above the soil. The CEL-models are discretized with 13,200, 88,320 and 1,412,160 elements.

Results

The reaction forces of the pile are shown in Figure 29. The reaction force in the SPH-simulations increases with decreasing mesh size. In contrast, the reaction force calculated in the CEL-simulations decreases with decreasing mesh size. The differences between the reaction forces of the fine and the very fine discretization show, that the SPH-method is applicable to simulation pile installation processes. The restriction of the SPH-method implemented in Abaqus is the required calculation time, because the method cannot yet be parallelized.

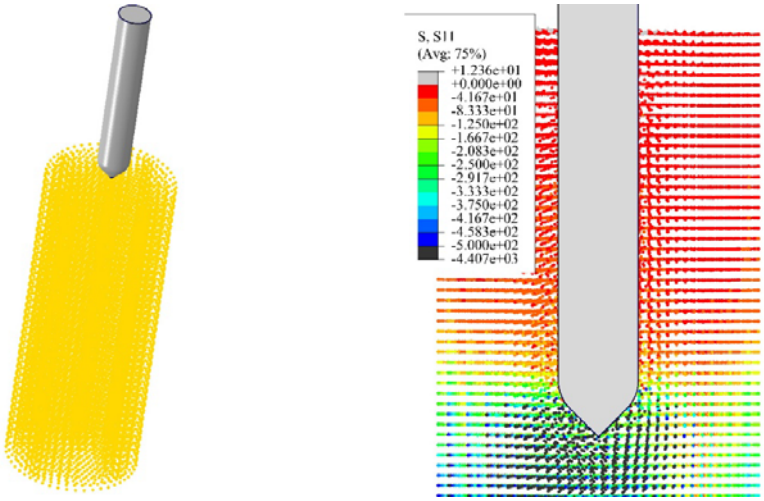

Figure 28. Numerical model (left) and deformed model with horizontal stresses (right).

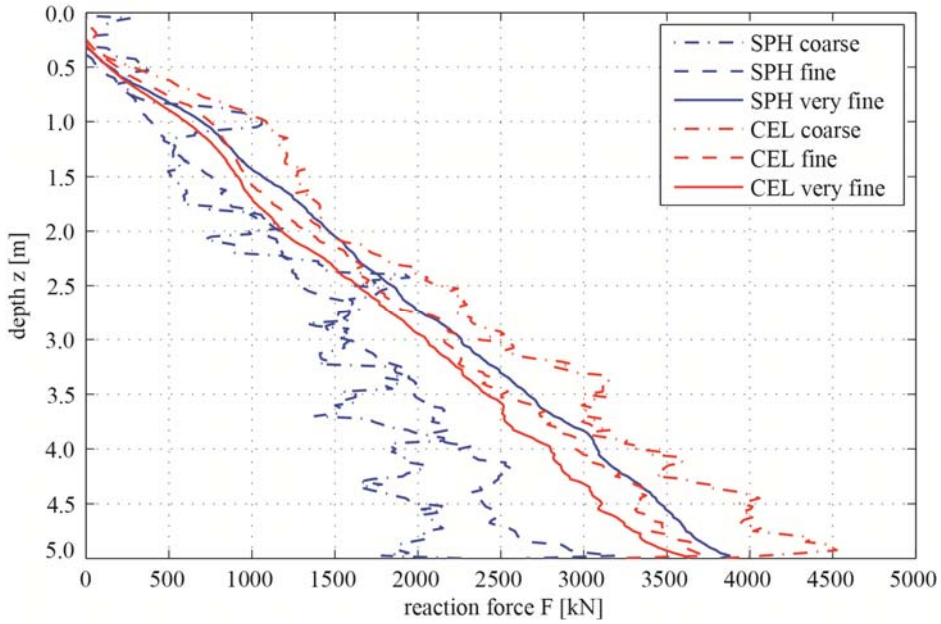

Figure 29. Reaction forces during the pile installation depending on the model discretization.

5. Conclusion

This paper shows a wide range of geomechanical examples for the numerical calculation of large deformation problems. The Finite-Element-Method, the coupled Eulerian-Lagrangian method and the smoothed particle hydrodynamics method are used for the simulations. Including the first sections of this paper, the complexity of geomechanical boundary problems is presented theoretically and with regard to computer simulations, especially the commercial code Abaqus.

It is shown, that Abaqus can be used for calculations of large deformation problems and is a powerful tool to evaluate the behaviour of the soil continuum under complex loading conditions.

For conclusions regarding a specific example, please refer to the corresponding section.

6. References

1. Arnold, A., “Zur Berechnung des Erd- und Auflastdrucks auf Winkelstützwände im Gebrauchszustand”, Promotionsschrift, Mitteilungen des Instituts für Geotechnik der TU Dresden, Heft 13, 2004.
2. Biehl, F., “Collision of ships with offshore wind turbines: Calculation and risk evaluation”, PhD Thesis, Institute for Ship Structural Design and Analysis, Hamburg University of Technology, 2008.
3. Busch, P., Grabe, J., Gerressen, F.W., and Ulrich, G., “Use of displacement piles for reinforcement of existing piles”, Proceedings of DFI and EFFC 11th Int. Conf. in the DFI series, Geotechnical Challenges in Urban Regeneration in London/UK, pp. 113-119, 2010.
4. Gudehus, G., “A Comprehensive Constitutive Equation for Granular Materials”, Soils and Foundations, 36(1): 1–12, 1996.
5. Gutjahr, S., “Optimierte Berechnung von nicht gestützten Baugrubenwänden in Sand”, Promotionsschrift, Schriftenreihe des Lehrstuhls Baugrund-Grundbau der Universität Dortmund, Heft 25, 2003.
6. Henke, S., “Herstellungseinflüsse aus Pfahlrammung im Kaimauerbau”, Dissertation, Veröffentlichungen des Instituts für Geotechnik und Baubetrieb der TU Hamburg-Harburg, Heft 18, 2008.
7. Henke, S., and Grabe, J., “Numerical modeling of pile installation”, Proc. of 17th Int. Conf. on Soil Mechanics and Foundation Engineering (ICSMFE), pp. 1321-1324, 2009.
8. Hill, R., “The mathematical theory of plasticity”, Clarendon Press, Oxford, 1950.
9. Lewis, R. W., and Schrefler, B. A., “The Finite Element Method in the Static and Dynamic Deformation and Consolidation of Porous Media”, Second Edition, Wiley Verlag, 2000.
10. Lysmer, J., and Kuhlemeyer, R. L., “Finite Dynamic Model for Infinite Media“, Journal of the Engineering Mechanics Division of the ASCE, pp. 859-877, 1969.
11. Mahutka, K.-P., “Zur Verdichtung von rolligen Böden infolge dynamischer Pfahleinbringung und durch Oberflächenrüttler.”, Dissertation, Veröffentlichungen des Instituts für Geotechnik und Baubetrieb der TU Hamburg-Harburg, Heft 15, 2007.

12. Mair, R. J. (1979). Centrifugal modelling of tunnel construction in soft clay. Phd thesis, Cambridge University, UK.
13. Meyerhof, G.G., “Bearing capacity of anisotropic cohesionless soils”, Canadian Geotecnical Journal, 15(4):592–5, 1978.
14. Niemunis, A., and Herle, I., “Hypoplastic Model for Cohesionsless Soils with Elastic Strain Range”, Mechanics of Cohesive-Frictional Materials, 2(4): 279–299, 1997.
15. Niemunis, A., “Extended hypoplastic models for soils”, Habilitationsschrift, Veröffentlichungen des Instituts für Grundbau und Bodenmechanik der Ruhr-Universität Bochum, Heft 34, 2003.
16. Qiu, G., and Grabe, J., “Explicit modeling of cone and strip footing penetration under drained and undrained conditions using a visco-hypoplastic model”, Geotechnik, 34:205-217, 2011.
17. Qiu, G., Henke, S., and Grabe, J., “Application of a Coupled Eulerian-Lagrangian approch on geomechanical problems involving large deformation”, Computers and Geotechnics, 38(1):30-39, 2011.
18. Qiu, G., and Henke, S., “Controlled installation of spudcan foundations on loose sand overlying weak clay”, Marine structures, 24(4):528-550, 2011a.
19. Qiu, G., and Grabe, J., “Numerical simulation of the deep penetration process of spudcans into sand overlying clay using the extended hypoplastic models”, Proceeding of the ISOPE Conference, 2012b.
20. Qiu, G., and Grabe, J., “Numerical investigation of the bearing capacity mechanisms due to spudcan penetration in sand overlying clay”, paper under review, 2012.
21. Schümann, B., “Modelling of soils as multi-phase materials with Abaqus”, Proceedings of SIMULIA Customer Conference 2010, Providence, USA, pp. 384-399, 2010.
22. Teh, K.L., Cassidy, M.J., Leung, C.F., Chow, Y.K., Randolph, M.F., and Quah, C., “Revealing the bearing capacity mechanisms of a penetrating spudcan through sand overlying clay”, Gèotechnique, 58(10):793–804, 2008.
23. Terzaghi, K., “Theoretical Soil Mechanics”, Second Printing, John Wiley and Sons Inc., New York, 1944.
24. Von Wolffersdorff, P.A., “A Hypoplastic Relation for Granular Materials with a Predefined Limit State Surface”, Mechanics of Cohesive-Frictional Materials, 1: 251–271, 1996.

7. Acknowledgment

The present work forms part of the research in the research training group “Seaports for Container-Ships of Future Generations” (GRK 1096) and the project “Finite element based multicriterial numerical optimization of geotechnical structures in the service limit state” (GR-1024-9-1), funded by the German Research Foundation (DFG). The funding is greatly appreciated.